Van de Velde, G., Nakai, S., Nakagawa, H. & Matoba, M. (2025), Dynamic behavior considering soil-structure interaction of a wharf at Corinto Port, Chinandega, Nicaragua, Synopsis of IISEE-GRIPS Master's Thesis, Bulletin of IISEE, 60

DYNAMIC BEHAVIOR CONSIDERING SOIL-STRUCTURE INTERACTION OF A WHARF AT CORINTO PORT, CHINANDEGA, NICARAGUA

VAN DE VELDE BLANDON German Jose[1]

Supervisors: Shoichi NAKAI[2]
Hiroto NAKAGAWA[2],
Moeko MATOBA[2]

ABSTRACT

Port facilities contribute to the economic development of countries and promote economic growth in the local area. There are between 6,000 and 7,000 ports worldwide, although only a few are relevant in the global context. Owing to their location, seaports are vulnerable to natural disasters, such as earthquakes, tsunamis, and typhoons. The main problems that appear after a natural disaster include soil liquefaction, crane collapse, and weakened joints connecting the decks and piles. In Central America, there are currently 12 essential port facilities, among them Corinto Port, which is the most important port in Nicaragua. Currently, there is no national seismic code for the construction of port facilities in Nicaragua. The goal of this study was to assess the dynamic behavior of seaport facilities by considering the soil structure interaction of a wharf at Corinto Port, Chinandega, Nicaragua. We utilized construction drawings, boreholes, seismic, and geophysical surveys to determine the material properties and geometry of a soil domain with the wharf structure. Additionally, we made use of OpenSeesPy to create the raw programming code. The results showed that the dynamic behavior of the soil domain varies with the wharf structure, ground motion characteristics (amplitude, phase, and frequency), and the quantity of energy of each event. The wharf structure was found to have undergone greater internal forces from short-duration, high-amplitude ground motion.

Keywords: Dynamic behavior, soil-structure interaction, wharf, port, ground motion.

1. INTRODUCTION

In the context of world trade, emerging economies are finding new ways to participate in global markets and promote economic growth. In this sense, basic economic infrastructure, including seaports, is key to the mobility of goods and services. There are between 6,000 and 7,000 ports in the world, although only a few hundred have significant importance in the global context. The countries of Central America, home to twelve seaports, have the geographic advantage of access to both the Atlantic and Pacific Oceans. The proximity to the Panama Canal is also an important advantage (SIECA, 2023). Many researchers have conducted soil-structure interaction analyses to evaluate the dynamic behavior of structures, following new seismic design guidelines (Chiou et al. 2011; Chiaramonte et al. 2013; Nakai and Nakagawa 2017; Su et al. 2017; Su et al. 2019; Vytiniotis et al. 2019; Özcebe et al. 2022; Plata et al. 2024). However, several developing countries do not have established seismic codes for port facilities and must adapt their designs based on the specifications from other countries. To the best of our knowledge, this investigation was directed toward evaluating the dynamic behavior considering the soil-structure interaction of a wharf at Corinto Port, Chinandega.

[1] Professor Researcher at the National Autonomous University of Nicaragua, Managua
[2] International Institute of Seismology and Earthquake Engineering, Building Research Institute

Approved as Master Paper of DMP by BRI/GRIPS

2. DATA

2.1. Target site

The target site of this study is Corinto Port, Chinandega, Nicaragua. Corinto is the largest and most important Port in Nicaragua, based on the volume of international cargo and the number of vessels serviced. Different geotechnical, seismic, and geophysical tests were conducted in the project area. Data, obtained by drilling works, such as standard penetration test (SPT), MASW, and geophysical tomography tests, revealed the presence of land reclamation backfill (top), medium to dense sand (medium), and weathered volcanic rock (bottom) layers. The shear wave velocity (Vs) was 200 m/s for the upper layers and 500 m/s for the bottom layer. The spatial distribution of the tests and geotechnical profile at Corinto Port is shown at the top and bottom of Figure 1.

The details of the engineering drawings of the wharf structure are shown in Figure 2. Here, it is possible to notice the presence of a steel pile, a corbel, a deck, and a wall. The piles are driven steel piles featuring a diameter of 1,060 mm, a thickness of 25.4 mm. The deck has 5,300 mm × 450 mm between the wall and pile 1 and 6,300 mm × 450 mm between piles 2, 3, and 4.

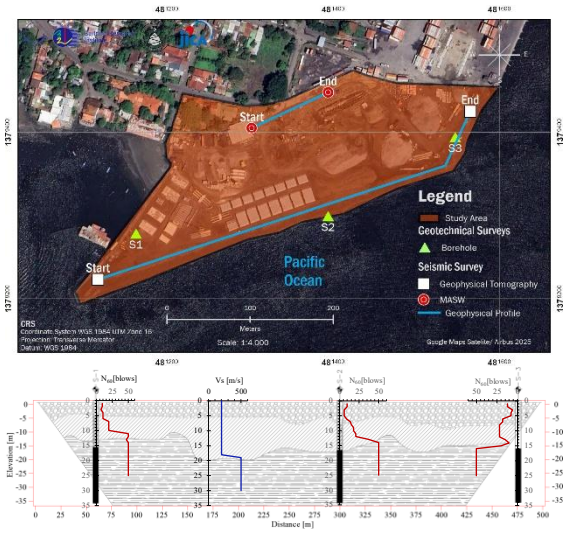

Figure 1. (Top) Spatial distribution of tests; (bottom) geotechnical profile at Corinto Port (Geological and Geophysical Institute, 2018, 2023)

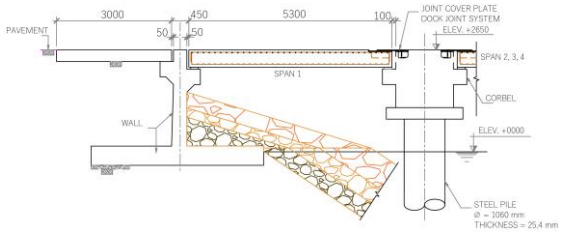

Figure 2. Cross-section of the wharf (National Port Authority, 2023)

2.2. Observed strong motion data

In this study, we used observed strong motion data from the Corinto seismic station provided by the Nicaraguan Institute for Territorial Studies (INETER), located at 3.5 km from the project area. A total of 18215 seismic events occurred from 2021 to 2023, with 43 having a magnitude greater than 5. So, two observed ground motions with different characteristics were selected. The 2022 Masachapa EQ is a long-duration event that occurred offshore, and the 2022 Estero Real River EQ is a short-duration event that occurred inland. The Pacific Earthquake Engineering Research Center (PEER) delivered the waveform of the 1972 Managua Earthquake (historical event) recorded by the Esso seismic station. Table 1 summarizes the general characteristics of seismic events considered in this study.

Table 1. General characteristics of seismic events.

Date	Time	Coordinates		Depth [km]	Mag.	Name	Seismic Station
		Lat. (deg)	Long (deg)				
2022/4/21	7:42:47	11.516	-87.03	35	6.6	Masachapa	Corinto
2022/9/6	7:35:34	12.936	-87.37	5	5.5	Estero Real River	Corinto
1972/12/23	6:29:43	12.33	-86.15	5	6.2	Managua	Esso

3. METHODOLOGY

3.1. Computational tools

In this study, several open-source programs, such as OpenSeesPy, ParaView, STERA WAVE, and ViewWave, were used to create raw programming codes, visualization, animation, scaled observation records, and a waveform analysis proposal.

3.2. Target geometry and material properties

The geometry of the numerical model considered in this study is shown in Figure 3, in which the following elements are visible: land reclamation layer (upper part), medium and dense sand (middle part), weathered volcanic rock (bottom part), and wharf structure. The seismic load was applied using horizontal dashpots located at the bottom of the model. The soil was modeled using elastic isotropic material, the piles using elastic material, and the dashpots using viscous materials. The location and distance between steel piles are shown, each pile having a diameter of 1,060 mm, a thickness of 25.4 mm, and a length of 23 m. The vertical component of the wharf is 3 m high and 0.4 m thick, while the horizontal component is 6 m long and 0.5 m thick. The deck is 0.45 m thick, and the spans are of the following lengths: span 1 is 6 m long, spans 2, 3, and 4 are 7 m. Both the wall and the deck are made of concrete. The geotechnical parameters assigned to the soil layers are listed in Table 5, while the mechanical properties of the structural components are shown in Table 3.

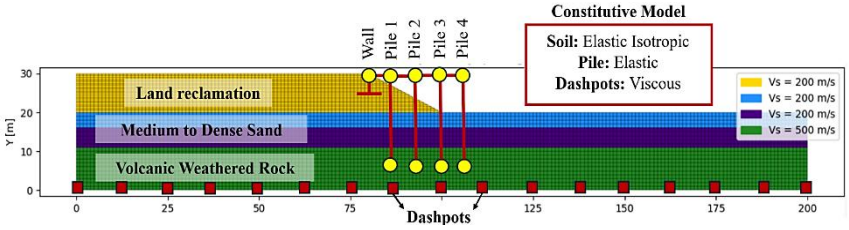

Figure 3. Geometry of the numerical model

Table 2. Material properties of the soil at Corinto Port

Depth [m]	Elevation [m]	Soil Layer	Thickness [m]	Density [kg/m^3]	Shear Modulus G [kg/m^2]	V_s [m/s]
10	30	Land Reclamation	10	1800	7.20E+07	200
13.5	20	Medium Sand	3.5	1600	6.40E+07	200
19	16.5	Dense Sand	5.5	1700	6.80E+07	200
30	11	Weathered Rock	11	2000	5.00E+08	500
-	-	Fractured Rock	-	2000	9.80E+08	700

Table 3. Properties of materials used in the structural system of the wharf

Material	Properties	Value
Concrete	Young Modulus (E)	4.70E+09 Pa
	Density (ρ)	2.40E+03 kg/m^3
	Compressive strength ($f'c$)	3.50E+07 Pa
Steel	Young Modulus (E)	2.05E+11 Pa
	Density (ρ)	7.90E+03 kg/m^3

3.3. Bedrock input ground motion

The observed ground motions were scaled using the response spectrum for Corinto Port, considering a Design Earthquake Level 2 Extreme with a return period greater than 1,000 years and a PGA greater than 0.6 g. Then, the deconvolution method using outcrop motion was applied, considering the influence

of the geometric irregularity of the ground surface. Two different bedrock input ground motions were derived from each seismic observation record, considering the soil thickness in the upland and lowland areas. The dynamic analysis was done at four points located at the ground surface (CP_1, CP_2, CP_3, and CP_4). Control points 1 and 4 are located on both sides of the slope, and control points 2 and 3 are situated at the top and bottom of the slope. In this study, the dynamic behavior considering soil structure interaction is analyzed using 2022 Masachapa EQ with M6.6. The bending moment and shear force envelopes were determined using all the seismic events. Figure 4 shows the sequence of the deconvolution method applied to the seismic records, along with the control points distributed on the ground surface.

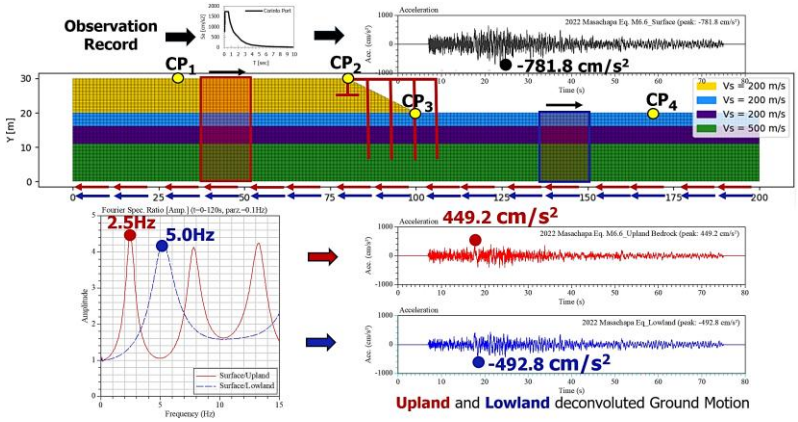

Figure 4. Deconvolution method applied to seismic records with ground-surface control points.

4. RESULTS AND DISCUSSION

4.1. Effect of bedrock deconvoluted ground motion

The PGA distribution of soil with the wharf structure under the influence of the upland and lowland deconvoluted 2022 Masachapa EQ with M 6.6 is shown in Figure 5. The numerical model with the upland-deconvoluted ground motion (left) displayed the maximum acceleration in the lowland region, and the numerical model with the lowland-deconvoluted ground motion (right) exhibited the maximum acceleration in the upland area, specifically at the top of the slope.

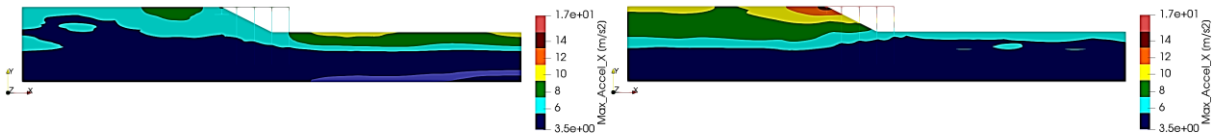

Figure 5. PGA in soil with a wharf structure, considering (left) upland, and (right) lowland deconvoluted ground motion

Comparison CP_1 and CP_4

The response of the soil with a wharf structure was determined at control points 1 and 4 using the Fourier amplitude (Figure 6). When the upland deconvoluted ground motion was applied (left), the lowland region was amplified, given that it vibrated at a natural frequency of 5 Hz. This frequency matches the maximum amplitude in the transfer function for the lowland region (see Figure 4). Additionally, when the lowland deconvoluted ground motion was applied (right), the upland region was amplified, as it vibrates at a natural frequency of 1.8 and 2.5 Hz. Accordingly, when the deconvolution method is applied to the upland region, the bedrock input ground motion amplifies the frequencies in this region. However, it is important to note that the lowland area is thinner and has a shorter fundamental period (higher frequencies), which generates resonance. Additionally, when the deconvolution method was applied to the lowland region, the bedrock input ground motion amplified the frequencies in this region.

Nevertheless, the upland area has greater thickness with a longer fundamental period (lower frequencies), generating resonance.

Comparison CP_2 and CP_3

The response of the soil with the wharf structure at control point 2 and control point 3 based on the Fourier amplitude is shown in Figure 6. When the upland deconvoluted ground motion is applied, the top and bottom of the slope have the same natural frequency, close to 1.8 Hz. This frequency does not match the maximum frequency in the transfer function for the upland and lowland regions. However, a second dominant peak, with a natural frequency of 2.5 Hz, matches the maximum frequency of the upland region in the transfer function. Therefore, the amplification phenomena were generated at control point 2 (top of the slope). In addition, when the lowland deconvoluted ground motion was applied, the top of the slope (control point 2) exhibited a natural frequency of 2.5 Hz. The bottom of the slope has a natural frequency of 1.8 Hz. The natural frequency obtained at the top of the slope matched the maximum frequency in the transfer function for the upland area. This can be attributed to the irregular surface complexity, slope geometry, and characteristics of each deconvoluted input ground motion.

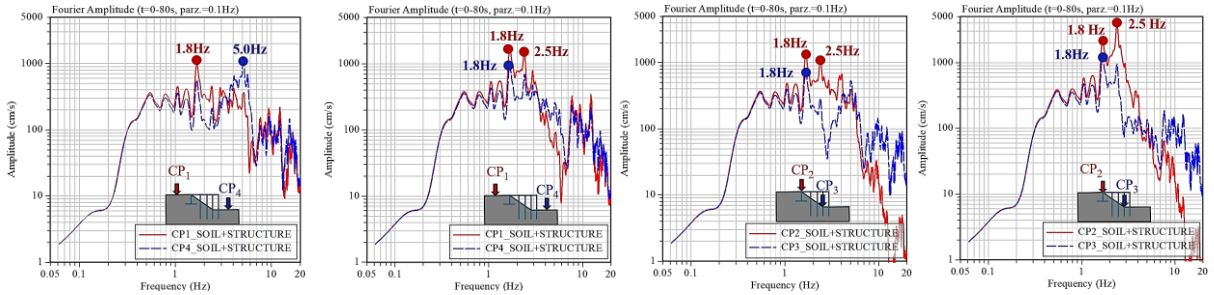

(upland) (lowland) (upland) (lowland)

Figure 6. Fourier amplitude in control points considering upland, and lowland deconvoluted ground motion

4.2. Internal forces

The plots shown in Figure 7 depict the shear force envelope (left) and bending moment envelope (right) considering lowland deconvoluted ground motion. The results revealed that the 2022 Estero Real River EQ M5.5 generated maximum shear forces and bending moment, and lowland deconvoluted ground motion was the most unfavorable condition. The maximum shear force appeared at the wall-deck joint and at the pile-deck joints, and it was decreasing from left to right. The maximum value of the bending moment was observed on the piles, and its distribution along the pile depends on its location. Maximum bending moment values were obtained in contact with the ground surface and due to the interaction between the weathered volcanic rock and the sand layer.

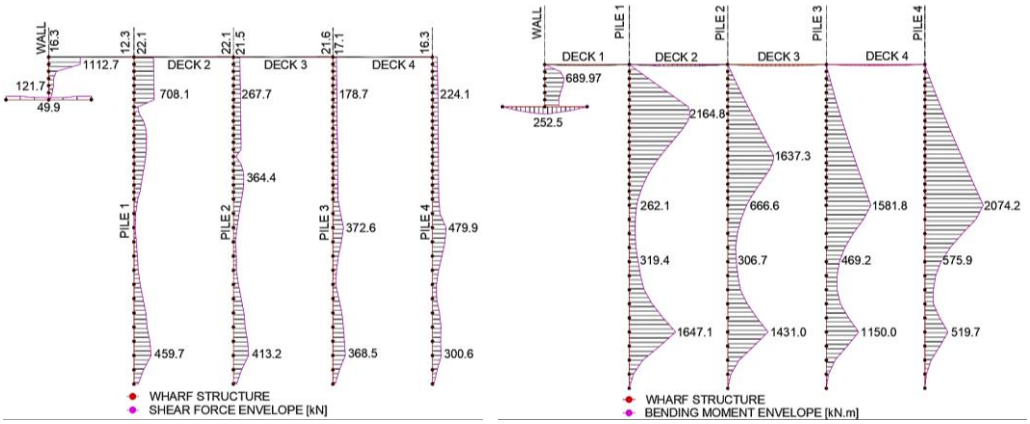

Figure 7. Internal Forces considering lowland deconvoluted ground motion (left) shear force envelope, (right) bending moment envelope

5. CONCLUSIONS

To advance the development of a new Nicaraguan Seismic Code for Port Structures, this study evaluated the dynamic behavior considering the soil-structure interaction of the wharf at Corinto Port, Chinandega, Nicaragua. Based on these results, we conclude the following:

When the response spectrum is considered on the ground surface, it is necessary to apply a deconvolution method to calculate the bedrock input ground motion. If the ground surface is irregular, the ground motion at the bedrock varies depending on soil thickness.

The upland and lowland deconvoluted ground motion modified the response of the soil and the soil with a wharf structure. The results demonstrated that the lowland deconvoluted ground motion had a significant impact on the displacements and internal forces of the wharf structure.

The wharf structure experienced greater internal forces for short-duration high-amplitude ground motions.

This study represents the first technical step toward developing a Seismic Design Code that strengthens the seismic resilience of the Nicaraguan Port infrastructure.

ACKNOWLEDGEMENTS

This research was conducted during the individual study period of the training course “Seismology, Earthquake Engineering and Tsunami Disaster Mitigation” by the Building Research Institute, JICA, and GRIPS. I wish to express my sincere gratitude to my thesis supervisor, Dr. Shoichi Nakai, for his continuous guidance, support, and valuable follow-up throughout this research. His mentorship played a crucial role in the successful completion of this work. I am also truly thankful to my advisors, Dr. Hiroto Nakagawa and Dr. Moeko Matoba, for their feedback, encouragement, genuine cooperation, and technical assistance during the development of this work.

REFERENCES

Chiou, J.-S., Chiang, C.-H., Yang, H.-H., & Hsu, S.-Y. (2011). Soil dynamics and earthquake engineering, 31(5-6), 830-840.

Chiaramonte, M. M., Arduino, P., Lehman, D. E., & Roeder, C. W. (2013). Earthquake Engineering & Structural Dynamics, 42(10), 1435–1450.

Geological and Geophysical Institute. (2018). Estudio de respuesta sísmica de sitio en Puerto Corinto, Departamento de Chinandega, Nicaragua.

Geological and Geophysical Institute. (2023). Estudio Geofísico para determinar espesor de horizontes y profundidad del estrato de AAA.

National Port Authority. (2023). Muro típico, plantas, cortes y detalles. In 101-NI-ID-EST-´Ñ-016 (Ed.).

Nakai, S., & Nakagawa, H. (2017). Procedia Engineering, 199, 2408-2413.

SIECA. (2023). Regional Master Plan 2035 on Mobility and Logistics.

Su, L., Lu, J., Elgamal, A., & Arulmoli, A. K. (2017). Soil Dynamics and Earthquake Engineering, 95, 167-179.

Su, L., Wan, H.-P., Bi, K., Li, Y., Lu, J., Ling, X.-Z., Arulmoli, A. K. (2019). Soil Dynamics and Earthquake Engineering, 122, 211-227.

Vytiniotis, A., Panagiotidou, A.-I., & Whittle, A. J. (2019). Soil Dynamics and Earthquake Engineering, 119, 21–35.

Özcebe, A. G., Bozzoni, F., & Borzi, B. (2022). Infrastructures, 7(8), 102.

Plata, R. R., Lai, C. G., & Cubrinovski, M. (2024). Japanese Geotechnical Society Special Publication, 10(15), 495-500.